Development 136, 2591-2600 (2009) doi:10.1242/dev.038448

The ENTH domain protein Clint1 is required for epidermal homeostasis in zebrafish

M. Ernest Dodd[1], Julia Hatzold[2], Jonathan R. Mathias[1], Kevin B. Walters[3], David A. Bennin[5], Jennifer Rhodes[4], John P. Kanki[4], A. Thomas Look[4], Matthias Hammerschmidt[2] and Anna Huttenlocher[1,3,5,*]

Epidermal hyperproliferation and inflammation are hallmarks of the human condition psoriasis. Here, we report that a zebrafish line with a mutation in the cargo adaptor protein Clint1 exhibits psoriasis-like phenotypes including epithelial hyperproliferation and leukocyte infiltration. Clint1 is an ENTH domain-containing protein that binds SNARE proteins and functions in vesicle trafficking; however, its in vivo function in animal models has not been reported to date. The *clint1* mutants exhibit chronic inflammation characterized by increased Interleukin 1β expression, leukocyte infiltration, bidirectional trafficking and phagocytosis of cellular debris. The defects in *clint1* mutants can be rescued by expression of zebrafish *clint1* and can be phenocopied with *clint1*-specific morpholinos, supporting an essential role for Clint1 in epidermal development. Interaction studies suggest that Clint1 and Lethal giant larvae 2 function synergistically to regulate epidermal homeostasis. Accordingly, *clint1* mutants show impaired hemidesmosome formation, loss of cell-cell contacts and increased motility suggestive of epithelial to mesenchymal transition. Taken together, our findings describe a novel function for the ENTH domain protein Clint1 in epidermal development and inflammation and suggest that its deficiency in zebrafish generates a phenotype that resembles the human condition psoriasis.

KEY WORDS: Epidermis, Zebrafish, Inflammation, Hemidesmosome

INTRODUCTION

The epidermis is a stratified epithelium that provides a crucial barrier against pathogens and other environmental insults. An essential function of the epidermis is to respond to physical insults with repair mechanisms that include wound healing characterized by regulated epithelial proliferation and leukocyte infiltration. A hallmark of epithelial disorders, including psoriasis and some epidermal cancers, is uncontrolled epithelial proliferation and inflammation. Although a genetic predisposition contributes to the development of psoriasis and other epidermal conditions, the precise molecular mechanisms that lead to the development of these heterogeneous disorders remain unknown and are likely to be multifactorial. Therefore it is essential to develop model systems to dissect pathways that regulate epidermal homeostasis and inflammation.

Recent studies indicate that the zebrafish represents a powerful model system with which to study mechanisms of epidermal development. The identification in zebrafish of homologs of human genes that are involved in epidermal tissues, such as *p63* (also known as *tp63* – ZFIN) (Bakkers et al., 2002; Lee and Kimelman, 2002), *rbp4* (Tingaud-Sequeira et al., 2006) and keratin isoforms (Imboden et al., 1997; Chua and Lim, 2000; Martorana et al., 2001; Thisse and Thisse, 2004), suggests that genetic conservation exists between zebrafish and mammals. Furthermore, the identification of mutants such as *hai1* (*spint1*) (Carney et al., 2007; Mathias et al., 2007), *penner* (*lgl2*) (Sonawane et al., 2005), *lama5* (Webb et al., 2007) and *psoriasis* (Webb et al., 2008) is providing more clues as to the genetic program of epidermal development in zebrafish.

The epidermis in developing zebrafish embryos contains two layers: a basal layer and a superficial layer of keratinocytes (Le Guellec et al., 2004). Adhesive structures that anchor the basal layer to the underlying basement membrane or mediate cell-cell contacts are essential for the integrity of epithelial tissues. A recent study reported that zebrafish Lethal giant larvae 2 (Lgl2; Llgl2) functions in the formation and maintenance of hemidesmosomes, and deficiency of Lgl2 results in loss of epidermal integrity in zebrafish (Sonawane et al., 2005). Additionally, the recently reported mutants *hai1* and *lama5* demonstrate abnormal cell-cell contacts and impaired epidermal integrity (Carney et al., 2007; Webb et al., 2007).

The zebrafish also provides a powerful model with which to study inflammation and leukocyte trafficking. The innate immune system is highly conserved in zebrafish (de Jong and Zon, 2005; Carradice and Lieschke, 2008), and they are used to study host-pathogen interactions (Davis et al., 2002; van der Sar et al., 2003; Pressley et al., 2005). Models of acute inflammation have been described using transgenic zebrafish that allow high-resolution observation of leukocyte recruitment (Mathias et al., 2006; Renshaw et al., 2006; Hall et al., 2007; Meijer et al., 2008). These reports demonstrate that acute inflammation in zebrafish involves the active recruitment of neutrophils into tissues, which can be resolved by reverse chemotaxis (Mathias et al., 2006).

To identify genes involved in inflammation, we screened a collection of zebrafish mutants for abnormal infiltration of neutrophils into the fin. Here we describe the *hi1520* line that was identified in this screen and carries an insertion in the *clathrin interactor 1* (*clint1*, also known as *enthoprotin* and *epsinR*) locus. Clint1 is an adaptor molecule in clathrin-mediated vesicular transport that binds membrane and clathrin coat components as well as cargo proteins, such as the vesicle-associated SNARE proteins

[1]Department of Medical Microbiology and Immunology, University of Wisconsin-Madison, Madison, WI 53706, USA. [2]Institute for Developmental Biology, Center for Molecular Medicine Cologne, and Cologne Excellence Cluster on Cellular Stress Responses in Aging-Associated Diseases, University of Cologne, Cologne, Germany. [3]Program in Cellular and Molecular Biology, University of Wisconsin-Madison, Madison, WI 53706, USA. [4]Department of Pediatric Oncology, Dana-Farber Cancer Institute, Boston, MA 02115, USA. [5]Department of Pediatrics, University of Wisconsin-Madison, Madison, WI 53706, USA.

*Author for correspondence (e-mail: huttenlocher@wisc.edu)

Accepted 21 May 2009

(v-SNAREs) involved in the vesicular fusion machinery (Kalthoff et al., 2002; Wasiak et al., 2002; Mills et al., 2003; Miller et al., 2007). However, previous studies have not addressed the function of Clint1 during the development of multicellular organisms.

Here we describe a novel function for Clint1 in epidermal development in zebrafish. *clint1* mutants exhibit epidermal aggregation, hyperproliferation and inflammation. Leukocytes display phagocytosis of cellular debris and robust bidirectional trafficking between epidermal tissues and the vasculature. Rescue and knockdown experiments confirm the contribution of *clint1* to these phenotypes. Furthermore, interaction studies suggest that Clint1 functions synergistically with Lgl2 to regulate epidermal homeostasis, and electron micrographs of *clint1* mutants demonstrate defects in hemidesmosome formation. Time-lapse microscopy demonstrates both a loss of cell-cell contact and increased motility of *clint1*-deficient epidermal cells, suggestive of epithelial to mesenchymal transition (EMT). Taken together, our findings describe a novel function for the ENTH domain protein Clint1 in epidermal development and suggest that its deficiency generates a phenotype in zebrafish that resembles the human condition psoriasis.

MATERIALS AND METHODS

Zebrafish maintenance

All zebrafish protocols were approved by the University of Wisconsin-Madison Research Animal Resources Center. Adult AB zebrafish and embryos were maintained (Nuesslein-Volhard and Dahm, 2002) and staged (Kimmel et al., 1995) as established. Wounding was performed as described (Mathias et al., 2006). The *clint1* allele *hi1520* was isolated in an insertional mutagenesis screen (Amsterdam et al., 1999) and is maintained in heterozygous adults. *hi1520* adults were crossed to *Tg*(*mpx:GFP*)^{uwm1} (Mathias et al., 2006) adults to yield *clint1;mpo:GFP* embryos. The *Tg*(*β-actin:hras-eGFP*) (allele *vu118*) line was described previously (Cooper et al., 2005).

RNA isolation and RT-PCR

Total RNA was isolated from single or pooled embryos using STAT-60 (Tel-Test). mRNA transcripts were detected using a one-step RT-PCR Kit (Qiagen). Primers for detection of levels and alternative splicing of transcripts were (5′-3′): *clint1*, AAAGTGCGGGAGCTGGTTGAT and GCCGTTCTCGTCGACACAATGAT; *il1b*, GCATGCGGGCAATATGAAGT and GTTCACTTCACGCTCTTGGATG (Pressley et al., 2005); *vti1b*, GACGAAGTGAAGTTGATGCCAGAAC and ATACCCTGAAGCACTTCTTCAGC; and *elongation factor 1 alpha* (*ef1a*), TACGCCTGGGTGTTGGACAAA and TCTTCTTGATGTATCCGCTGAC. The exon trap in *clint1* was identified with primer set (5′-3′): AAGGATTACAAGGACGACGA (Chen et al., 2002) and GCCGTTCTCGTCGACACAATGAT.

Whole-mount in situ hybridization

Embryos obtained from *hi1520* adults were raised in 0.2 mM N-phenylthiourea in E3 medium and fixed in 4% paraformaldehyde (PFA) in PBS. *mpo* and *clint1* mRNAs were labeled by whole-mount in situ hybridization (WISH) as described (Hammerschmidt et al., 1996; Bennett et al., 2001). A 1 kb fragment from the zebrafish *clint1* cDNA clone (accession no. BC085520, ATCC) was used to synthesize antisense DIG-labeled riboprobes. Combined colorimetric WISH and immunostainings were performed as described (Hammerschmidt et al., 1996; Carney et al., 2007).

Whole-mount immunolabeling, Acridine Orange staining and quantification

Zebrafish embryos were fixed and permeabilized as described (Mathias et al., 2006). Antibodies and dilutions used were: anti-p63 (1:300, Novus Biologicals; 1:200, Santa Cruz Biotechnology), anti-BrdU (1:100, Sigma), FITC anti-BrdU (1:300, Roche), anti-Mpo (1:300) (Mathias et al., 2006), anti-L-plastin (1:300) (Mathias et al., 2007), pan-cadherin (1:300, Sigma), pan-cytokeratin 1-8 (1:10, Progen Biotechnik) (Sonawane et al., 2005), anti-Pkcζ (1:200, Santa Cruz SC-216), FITC donkey anti-rabbit IgG (1:300, Jackson ImmunoResearch), Rhodamine Red X goat anti-mouse IgG (1:500, Molecular Probes), Rhodamine Red X goat anti-mouse Fab fragment (1:300, Jackson ImmunoResearch), Cy3 anti-mouse IgG (1:200, Invitrogen) and Alexa Fluor 488 goat anti-rabbit IgG (1:200, Invitrogen). DAPI staining was performed with a 1:1000 dilution of DAPI (1 mg/ml) in PBS. BrdU incorporation (Sonawane et al., 2005), Mpo/L-plastin double-immunolabeling and Acridine Orange (AO) staining (Walters et al., 2009) were performed as described. Co-immunolabeling of BrdU and p63 was performed as described (Lee and Kimelman, 2002), except that a Rhodamine Red X goat anti-mouse Fab fragment secondary antibody was used. Quantifications of BrdU, AO, displaced Mpo and displaced L-plastin were performed for representative experiments with at least 19 embryos per group. A box was duplicated onto each image in MetaMorph to ensure equivalency of the areas sampled. BrdU and AO signals were scored within the caudal fin fold within the boxed region. Displaced Mpo and L-plastin included all signals outside of the caudal hematopoietic tissue. Statistical analysis was performed in Prism (GraphPad) using paired two-tailed Student's *t*-tests with a 95% confidence interval and significance at $P<0.05$.

Zebrafish embryo sectioning

Unstained embryos or WISH-labeled embryos were fixed in 4% PFA, washed in PBS, suffused in 30% sucrose, embedded in paraffin and sectioned. Hematoxylin and Eosin staining was as described (Hsu et al., 2004). Immunolabeled embryos were post-fixed in 4% PFA, dehydrated through an ethanol series to 100% ethanol, embedded in Durcupan (Sigma) and sectioned.

Neutrophil tracking

Neutrophils from *clint1;mpo:GFP* embryos were tracked and analyzed as described (Mathias et al., 2006). Percentages of time stopped and directionality index (D/T) were calculated as described (Mathias et al., 2007). Data were collected from movies of three mutant embryos before (*clint1* mutant) and after (*clint1* post-wound) wounding of the caudal fin. For *clint1* post-wound cell tracks (n=22 from three fish), data include points from the onset of migration to the arrival at the wound (average duration of 27 minutes). For *clint1* mutant cell tracks (n=39 from three fish), data for percentages of time stopped include all points, and directionality data are derived from the first 27 minutes of each time-lapse. Data are presented as averages of three separate experiments.

Rescue studies

Zebrafish *clint1* cDNA was subcloned into pcDNA3.1 (Invitrogen), and *clint1* mRNA was synthesized using mMessage Machine (Ambion). Embryos obtained from *hi1520* adults were injected at the 1- to 2-cell stage with 0.5 pl *clint1* mRNA (150 or 250 ng/μl) or nuclease-free H_2O (control). Statistical analysis was performed in Prism (GraphPad) using one-way ANOVA with Tukey's multiple comparison post-hoc test with significance at $P<0.05$.

Morpholino oligonucleotide microinjection

Morpholino oligonucleotides (MOs) (GeneTools) were resuspended in 1× Danieau Buffer at a stock concentration of 1 mM. Final MO concentrations (below) were injected into the cell or yolk of 1- to 4-cell stage embryos. MO volumes and concentrations used were (5′-3′): standard control MO, 0.5 nl of 500 μM (GeneTools); *pu.1* MO, 1 nl of 1 mM (Rhodes et al., 2005); *clint1*-atg MO, 0.5 nl of 600 μM (CCGCACTTTCCACATATTCAACATC); *clint1*-ex1 MO, 0.5 nl of 400 μM (ACATCCAAAATACTCACGCTTTATC); *vti1b*-atg, 0.5 nl of 700 μM (TCAAACTCCTCTGAAGACATAGTGG); and *vti1b*-ex1, 0.5 nl of 250 μM (ATAAAGAGTTTATTCACCTCCCTGG). MOs for interaction studies were: 1.0-1.5 nl of both *clint*-ex1 (22 μM) and *lgl2* (22 μM; GCCCATGACGCCTGAACCTCTTCAT) (Sonawane et al., 2005). For injection into 8- to 32-cell embryos (see Fig. 5G,H), single cells were injected with 66 pl of cell tracer dye, 10 mg/ml tetramethyl Rhodamine-conjugated dextran (TMRD, Molecular Probes) or 500 μM *clint1*-atg MO in TMRD.

Expression analysis of *clint1* and *vti1b*

A fusion construct with mCherry (5′), obtained from Dr R. Tsien (University of California, San Diego, CA, USA), and *clint1* cDNA (3′) was cloned into a Tol2 construct (Walters et al., 2009). Tol2/CMV:mCherry-*clint1* DNA (25 ng) and transposase mRNA (45 ng) were co-injected at the 1-cell stage in a total volume of 1 nl, and in vivo confocal imaging was performed at 2 days post-fertilization (dpf) with a 60× water immersion objective and a 4.8× digital zoom. The *vti1b* cDNA clone (accession no. BC055131, ATCC) was subcloned into the eGFP-C1 vector (Clontech). Co-expression and imaging of mCherry-*clint1* and *vti1b*-GFP in HEK293 cells were performed as described (Doan and Huttenlocher, 2007).

Cell transplantations

One to four cells from *Tg*(*β-actin:hras-eGFP*) donors were transplanted into non-transgenic hosts to obtain clusters of GFP-labeled basal keratinocytes as described (Carney et al., 2007). Transplants (wild-type donor into wild-type recipient; *clint1* morphant donor into wild-type recipient) were used to assay the autonomy of the *clint1* mutant proliferation phenotype, and GFP-positive cells were counted at 2 and 3 dpf. Homotypic transplants (wild-type donor into wild-type recipient; *clint1* morphant donor into *clint1* morphant recipient) were used to image the behavior of keratinocytes in wild-type or *clint1* mutant environments. Recipients were allowed to develop to 36 hours post-fertilization (hpf), mounted and analyzed by time-lapse confocal microscopy as described (Carney et al., 2007). GFP-labeled keratinocytes in wild-type or *clint1* mutant environments were tracked using ImageJ (v1.41) and the MTrackJ plug-in. Statistical analysis was performed in Prism (GraphPad) using paired two-tailed Student's *t*-tests with significance at $P<0.05$.

Transmission electron microscopy

Tissues were fixed in 2.5% glutaraldehyde/2% PFA in PBS (0.1 M, pH 7.4) overnight at 4°C, or in 4% PFA overnight at 4°C followed by incubation in 2% glutaraldehyde in PBS for 2 hours at 4°C. Samples were post-fixed in 1% osmium tetroxide in PBS for 2 hours, dehydrated through an ethanol series, further dehydrated in propylene oxide, embedded in Durcupan, sectioned with an ultramicrotome (Leica) and contrasted with Reynolds lead citrate and 8% uranyl acetate in 50% ethanol. Ultrathin sections were observed with a Philips CM120 electron microscope, and images were captured with a MegaView III side-mounted digital camera.

Imaging

Images were captured with a Nikon SMZ-1500 zoom microscope, a Nikon Eclipse TE300 inverted microscope, an Olympus FV1000 FV10-ASW or Zeiss LSM710 laser-scanning confocal microscope. Embryos were anesthetized during image acquisition in 0.1 mg/ml Tricaine in E3 at 28°C. Color images were captured with NIS Elements D 2.30 software. All other 2D images were captured and analyzed with MetaMorph software. Confocal images were captured and rendered with Fluoview FV10-ASW software (v01.07).

RESULTS

An insertion in the zebrafish *clint1* locus causes epidermal defects and inflammation

To identify genes that are involved in regulating inflammation, a collection of zebrafish insertional mutants (Amsterdam et al., 1999) was screened at 2.5 dpf by WISH for expression of the neutrophil-specific myeloperoxidase (*mpo*, also known as *mpx*) gene (Bennett et al., 2001; Lieschke et al., 2001). Three of 276 lines screened displayed abnormal tissue distributions of neutrophils. Two of these lines, *hi2217* and *hi1019*, have been characterized (Carney et al., 2007; Mathias et al., 2007; Walters et al., 2009), and here we describe the third line, *hi1520*, with infiltration of neutrophils into the fin (Fig. 1F,F′). The retroviral insertion in the *hi1520* line was mapped to the intron between the first two coding exons of the *clint1* locus (Fig. 1A) (Amsterdam et al., 2004), and embryos with the *hi1520* insertion have alternatively spliced *clint1* transcripts due to an exon trap, as previously discussed (Amsterdam and Hopkins, 2004). Embryos homozygous for this insertion (*clint1* mutants) have reduced full-length *clint1* transcripts and display inflammatory phenotypes with increased expression of the inflammatory cytokine *il1b* (Fig. 1B). In addition, developmental defects of *clint1* mutants include embryonic lethality, smaller body size, pericardial edema, unconsumed yolk and impaired development of the liver and gut (Amsterdam et al., 2004).

The tissue distribution of *clint1* was determined by WISH for *clint1* mRNA and revealed predominant expression at 36 hpf within the epidermis (Fig. 1C-E), including the fin fold (Fig. 1C,E) and the lateral epidermis covering the trunk (Fig. 1C,D). *clint1* expression

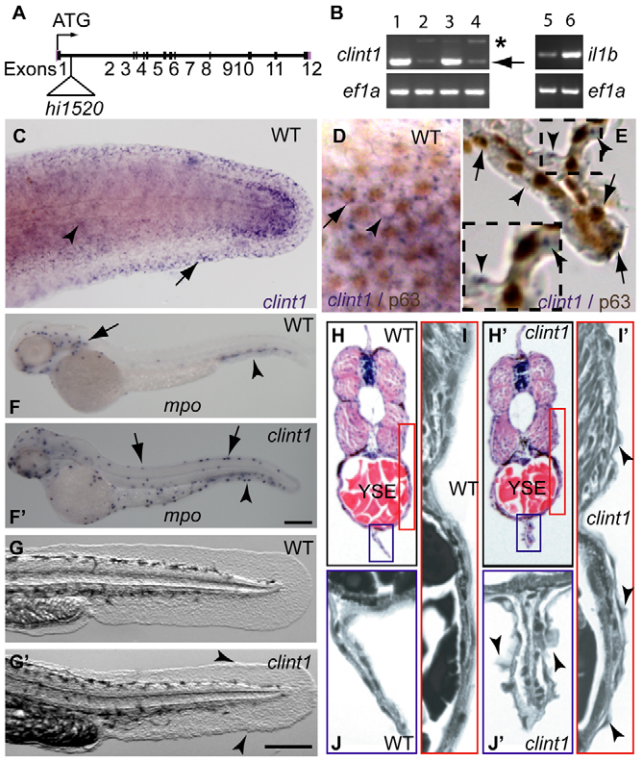

Fig. 1. Expression of *clint1* in epidermal tissues and reduced *clint1* expression, inflammation and epidermal defects in *hi1520* mutants. (**A**) Zebrafish *clint1* locus showing the *hi1520* insertion. (**B**) RT-PCR amplification of *clint1*, *il1b* and *ef1a* from wild-type embryos (1) and from heterozygous (3,5) and homozygous (2,4,6) *clint1* mutant embryos. Arrow and asterisk indicate full-length and alternatively spliced *clint1* transcripts, respectively. (**C-E**) Whole-mount in situ hybridization (WISH) of *clint1* (purple) in wild-type (WT) embryos at 36 hpf showing epidermal expression. (C) *clint1* expression within lateral epidermis (arrowhead) and fin fold (arrow). Lateral view (D) and transverse sections (E) of embryos subjected to WISH for *clint1* (purple) and p63 immunolabeling (brown) showing *clint1* expression in both p63-positive (arrows) and p63-negative (arrowheads) cells. (**F**,**F′**) WISH of *mpo* in wild-type (F) and in *clint1* mutant (F′) embryos. (F) Anterior (arrow) and posterior (arrowhead, CHT) hematopoietic tissues of wild-type sibling. (F′) Dorsal ridge (arrows) and caudal fin fold (arrowhead) of *clint1* mutants. (**G**,**G′**) Wild-type (G) and *clint1* mutant (G′) embryos at 48 hpf showing cellular aggregates (arrowheads). (**H-J′**) Hematoxylin and Eosin-stained transverse sections taken anterior to cloaca of wild-type (H-J) and *clint1* mutant (H′-J′) embryos at 48 hpf. Red and blue boxed regions in H,H′ are magnified in I,I′ and J,J′, respectively. Arrowheads (I′,J′) identify protruding epidermal cells. YSE, yolk sac extension. Scale bars: 200 μm.

was detected in both p63-positive and p63-negative cells of the epidermis (Fig. 1D,E). Consistent with the epidermal expression of *clint1*, *clint1*-deficient mutants displayed an abnormal fin morphology, with epithelial aggregates at 48 hpf (Fig. 1G,G′), allowing the earliest reliable sorting of mutants from wild-type siblings. Further examination of embryos at 48 hpf by transverse paraffin sectioning showed that epidermal aggregates of *clint1* mutants protruded from the epidermal sheet, especially in the fin fold (Fig. 1H′,J′) and the lateral epidermis covering the trunk and yolk sac extension (Fig. 1H′,I′), as compared with control embryos (Fig. 1H-J). Thus, our findings suggest a novel role for Clint1 in regulating epidermal morphology.

clint1 mutants exhibit epidermal hyperproliferation, cell death and inflammation

To determine whether epithelial aggregates are associated with cell proliferation, BrdU pulse-labeling was combined with anti-p63 staining to identify basal keratinocytes in control and mutant embryos. Mutants exhibited significantly increased BrdU labeling within both p63-positive and p63-negative cells of the epidermis at 48 hpf (Fig. 2A,A′,D), indicating epithelial hyperproliferation. The p63 staining highlighted morphological abnormalities of mutant cells along the edges of the caudal fin fold; mutants showed flattened, aggregated cells in comparison to the rounded and ordered appearance of these cells in wild-type siblings (Fig. 2A,A′). Proliferating cells were found dispersed throughout the fin fold and within the epidermal aggregates (Fig. 2A′). Similarly, AO staining was increased throughout the mutant fin fold at 48 hpf (Fig. 2B,B′,E), suggesting an increase in epidermal cell death. A time course showed significant elevations in epidermal proliferation and cell death in *clint1* mutants as early as 36 hpf (see Fig. S1A-F in the supplementary material); however, leukocyte infiltration was not observed in *clint1* mutants until 48 hpf (Fig. 2C′). Quantification of neutrophils outside the caudal hematopoietic tissue (CHT) revealed that *clint1* mutants have statistically significant neutrophil displacement as compared wild-type siblings (Fig. 2F). Together, the findings demonstrate that *clint1* mutants display enhanced proliferation, cell death and leukocyte infiltration.

clint1 mutants display persistent inflammation in epidermal tissues

The *clint1* mutant was identified by a chronic inflammation phenotype characterized by leukocyte infiltration in the fin (Fig. 1F′) and increased *il1b* expression (Fig. 1B). To further characterize the inflammation in *clint1* mutants, embryos were co-immunolabeled with antibodies to Mpo and L-plastin (Lcp1), a general leukocyte marker (Meijer et al., 2008). In *clint1* mutants at 48 hpf, two populations of cells – L-plastin-positive/Mpo-positive (neutrophils) and L-plastin-positive/Mpo-negative (macrophages and other leukocytes) – were observed throughout the epidermis, including the fin fold (Fig. 3A′,B′), the retinal pigment epithelium (data not shown) and the epidermis covering the trunk (Fig. 3B′). In wild-type siblings, leukocytes were excluded from these areas (Fig. 3A,B). Additionally, inflammation was not affected by raising the embryos in sterile E3 versus E3 containing *Escherichia coli* (see Fig. S2F in the supplementary material), suggesting that the inflammation phenotype was not affected by changes in bacterial load. Together, these findings indicate that *clint1* mutants have chronic inflammation associated with impaired epidermal homeostasis.

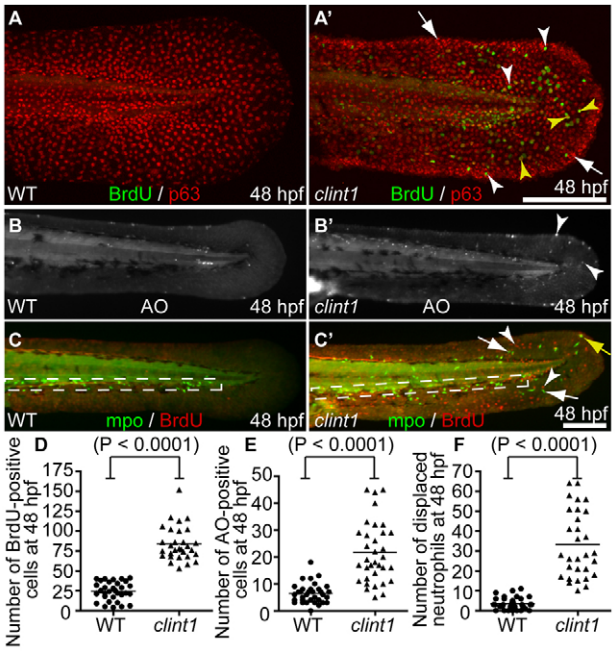

Fig. 2. *hi1520* mutant phenotypes at 48 hpf. (**A-C′**) Wild-type (A-C) and *clint1* mutant (A′-C′) 48 hpf zebrafish embryos labeled for BrdU incorporation (green) and p63 (red) (A,A′), Acridine Orange (AO) (B,B′) or Mpo (green) and BrdU incorporation (red) (C,C′). Boxed region, caudal hematopoietic tissue (CHT). Arrowheads identify proliferation in p63-positive (yellow arrowheads) and p63-negative (white arrowheads) cells (A′,C′), and cell death (B′) in *clint1* mutants. Arrows identify epidermal aggregates (A′) and neutrophils (C′) in *clint1* mutants. Yellow arrow (C′) identifies a proliferating neutrophil. (**D-F**) Quantification of BrdU (D) and AO (E) in fin fold and overall displacement of neutrophils (F) in wild-type (circles) and *clint1* mutant (triangles) embryos. Bars represent the mean. Scale bars: 200 μm.

Leukocytes exhibit phagocytosis of cellular debris and bidirectional trafficking in *clint1* mutants

To explore the dynamic properties of inflammation in vivo, the *clint1* mutant line was crossed with the *mpo:GFP* transgenic line (Mathias et al., 2006). Time-lapse images of *clint1;mpo:GFP* mutant larvae at 3 dpf revealed extensive infiltration of highly motile leukocytes within the epidermis. The leukocytes also displayed phagocytosis of cellular debris (Fig. 3C,D; see Movie 1 in the supplementary material). Time-lapse imaging and cell tracking of leukocyte motility in the *clint1* mutants at 3 dpf showed that the spontaneous leukocyte migration in the fin was characterized by periods of random motility alternating with frequent pauses (moving <0.75 μm/minute an average of 28% of the time; see Fig. S2A in the supplementary material). Neutrophils also displayed robust bidirectional trafficking between the epidermal tissues and the vasculature in the *clint1* mutant, suggesting that reverse migration and resolution were not impaired (see Fig. S2D and Movie 2 in the supplementary material). Neutrophil motility in mutants showed reduced cell velocity (5.7 μm/minute) and low directional persistence (0.4) as compared with the directed neutrophil response to wounding (8.3 μm/minute, average D/T=0.67; see Fig. S2B,C,E and Movie 3 in the supplementary material). Our findings indicate that neutrophils in *clint1* mutants retain the ability to respond to tissue wounding. Taken together, these findings demonstrate that

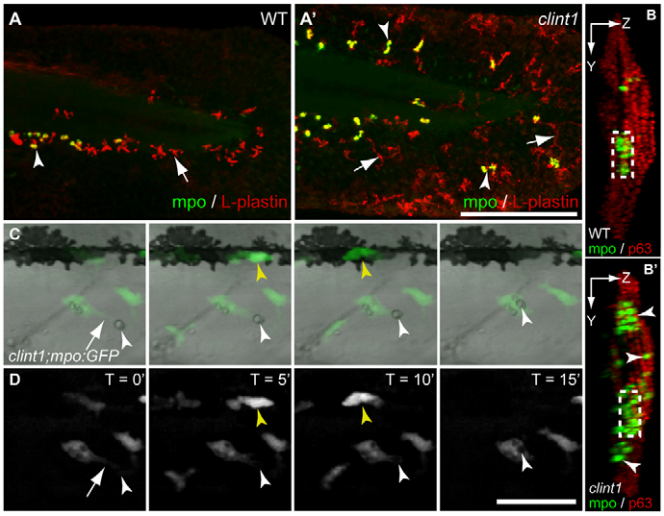

Fig. 3. Leukocyte infiltration of epidermis and phagocytosis of debris in *clint1* mutants. (**A-B′**) Wild-type (A,B) and *clint1* mutant (A′,B′) zebrafish embryos immunolabeled at 48 hpf for Mpo (green, arrowheads) and L-plastin (red, arrows) (A,A′) or for Mpo (green, arrowheads) and p63 (red) (B,B′). (A,A′) Mpo-expressing cells also express L-plastin and appear yellow. Leukocytes in *clint1* mutants infiltrate the caudal fin fold (A′,B′), the lateral epidermis covering the trunk (B′) and dorsal ridge (A′,B′). (B,B′) Confocal *yz* projections oriented with left side of the embryo facing to the right, dorsal up. Boxed region, CHT. (**C**,**D**) Overlay (C) and fluorescence stills (D) from time-lapse movie showing phagocytosis of cellular debris (white arrowhead) by a macrophage (arrow) in lateral epidermis of *clint1* mutant at 3 dpf (see Movie 1 in the supplementary material). Yellow arrowhead identifies a neutrophil. Scale bars: 200 μm in A′; 50 μm in D.

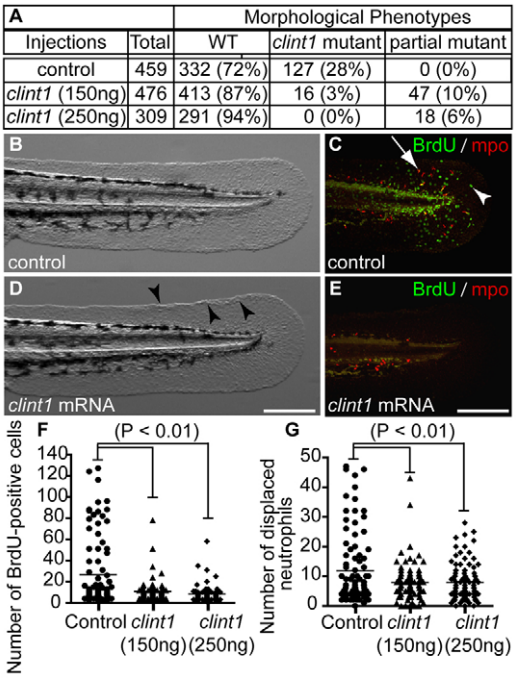

Fig. 4. Rescue of proliferation and inflammation by *clint1* mRNA overexpression in *clint1* mutants. (**A-E**) Data (A) and representative images of control-injected mutants (B,C) and *clint1* mRNA-injected partial mutants (D,E) that were immunolabeled for BrdU (green, arrowhead) and Mpo (red, arrow) (C,E). Arrowheads (D) identify epidermal aggregation. (**F**,**G**) Quantification of proliferation (F) and neutrophil displacement (G) in control-injected (circles) and *clint1* mRNA-injected (triangles, 150 ng/μl; diamonds, 250 ng/μl) embryos. Bars represent the mean. Scale bars: 200 μm.

leukocytes in *clint1* mutants display robust phagocytosis of cellular debris and bidirectional trafficking between the epidermal tissues and vasculature.

Clint1 mediates the *hi1520* mutant phenotype

To directly implicate Clint1 in the *hi1520* mutant phenotype, we determined whether ectopic expression of wild-type *clint1* mRNA could rescue the epidermal phenotype of *clint1* mutants. Control-injected embryos yielded 28% with *clint1* mutant phenotypes (Fig. 4A-C), close to the predicted Mendelian ratio of 25%, whereas clutches injected with two different concentrations of *clint1* mRNA (150 or 250 ng/μl) yielded increased numbers of embryos with wild-type morphology (87% or 94%, respectively), few with *clint1* mutant phenotypes (3% or 0%) and some with a partial rescue phenotype (10% or 6%) (Fig. 4A,D,E). There appeared to be a dosage-dependent effect of *clint1* mRNA expression on the morphological phenotype. Ectopic expression of *clint1* mRNA in the mutant background also significantly reduced inflammation and hyperproliferation (Fig. 4E-G).

To further implicate *clint1* in the epidermal phenotypes of *hi1520* mutants, morpholinos (MOs) were used to deplete wild-type embryos of Clint1. *clint1*-specific MOs targeted to the translational start site (*clint1*-atg MO) or the splice donor site of intron 1 (*clint1*-ex1 MO) (Fig. 5E) recapitulated the *hi1520* mutant phenotypes (Fig. 5A′,B,C′,D; see Fig. S3 in the supplementary material), whereas a standard control MO (con MO) had no effect (Fig. 5A-D; see Fig. S3 in the supplementary material). RT-PCR analysis with primers targeted to exons 1 and 4-5 (Fig. 5E) revealed that injection of *clint1*-ex1 MO reduced the amount of full-length *clint1* mRNA to below the detection threshold (Fig. 5F). Both *clint1*-atg and *clint1*-ex1 MOs induced epidermal hyperproliferation and aggregation of p63-positive cells by 36 hpf (Fig. 5A′,B), similar to *clint1* mutants. However, in contrast to *clint1* mutants, neutrophilic inflammation was evident in *clint1* morphants by 36 hpf (Fig. 5C′,D). We were unable to determine whether cell death was also an early feature of the *clint1* morphant phenotype at 36 hpf because control morphants exhibited significant increases in AO staining compared with uninjected wild-type embryos (data not shown). These findings demonstrate that the *clint1* morphant phenotype is similar to that of *clint1* mutants and support the genetic contribution of *clint1* to these phenotypes.

Clint1 localizes to intracellular vesicles

Recent work has shown that Clint1 interacts with SNAREs, such as Vti1b and syntaxins, to regulate clathrin-mediated vesicular trafficking (Wasiak et al., 2002; Chidambaram et al., 2008). Ectopically expressed zebrafish Clint1 was observed in intracellular vesicles in zebrafish epidermal cells (see Fig. S4A and Movie 4 in the supplementary material), and the zebrafish Clint1 and Vti1b isoforms were found to co-localize at intracellular vesicles in HEK293 cells (see Fig. S4B-D in the supplementary material). These data suggest a conserved function between the zebrafish and human Clint1 and Vti1b pathways; however, *vti1b* morphants

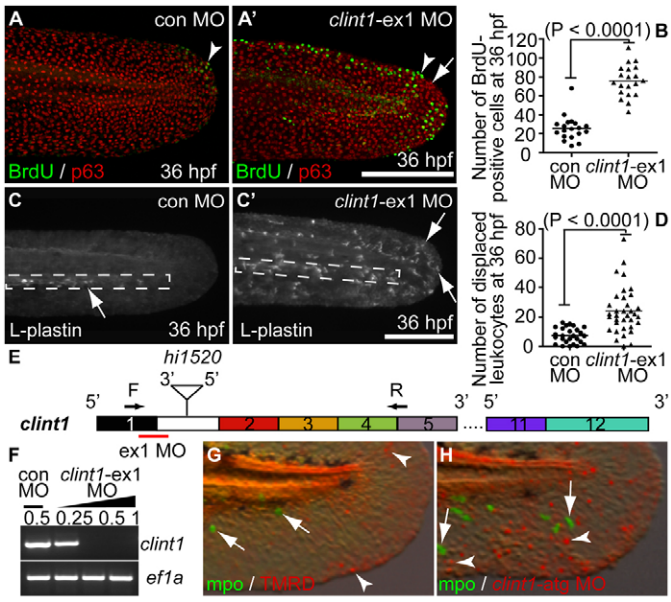

Fig. 5. *clint1* MOs phenocopy *hi1520* mutant phenotypes. (**A**,**A′**,**C**,**C′**) Zebrafish embryos immunolabeled at 36 hpf for BrdU incorporation (green) and p63 (red) (A,A′) or L-plastin (C,C′) following injection of control or *clint1*-ex1 MO into wild-type embryos. Arrowheads identify proliferative epidermal cells. Arrows identify epidermal aggregation (A′) and leukocytes (C,C′). Boxed region, CHT. (**B**,**D**) Quantification of proliferation (B) and leukocyte displacement (D) in control (circles) and *clint1*-ex1 MO-injected embryos (triangles). Bar represents the mean. (**E**) *clint1* exon structure and primers used to investigate alternative splicing. (**F**) RT-PCR amplification of *clint1* and *ef1a* from control and *clint1*-ex1 MO-injected wild-type embryos. (**G**,**H**) Embryos immunolabeled at 48 hpf for Mpo (green, arrows) following asymmetric injection of TMRD (G, arrowheads) or *clint1*-atg MO with TMRD (H, arrowheads) into single cells at the 8- to 32-cell stage. Scale bars: 200 μm.

showed no epidermal defects (see Fig. S4E,H-L in the supplementary material). Taken together, our findings implicate Clint1-mediated vesicular trafficking in the regulation of epidermal homeostasis.

Inflammation and proliferation are secondary phenotypes in *clint1* mutants

The timing of inflammation in *clint1* mutants suggests that it is a secondary phenotype. To determine whether inflammation causes the epithelial defects, *clint1* mutants were injected with MOs specific for *pu.1* (*spi1*) to inhibit myeloid lineage development (Rhodes et al., 2005) (see Fig. S5 in the supplementary material). The *pu.1* MO blocked the development of macrophages and neutrophils in *clint1* mutants without preventing epidermal aggregation (see Fig. S5C′ in the supplementary material) or hyperproliferation (see Fig. S5D′ in the supplementary material). Limited efficacy of the *pu.1* MO after 2 dpf prevented an assessment of the role of leukocytes in the progression of the fin phenotype at later stages. These findings suggest that the induction of the epithelial phenotypes in the *clint1* mutants is independent of leukocyte infiltration.

To address the relationship between epidermal aggregation and inflammation, we knocked down Clint1 in a subset of embryonic cells and monitored the distribution of neutrophils. Tracer dye, TMRD, or *clint1*-atg MO with TMRD, was injected into single cells of embryos at the 8- to 32-cell stage to facilitate asymmetric distribution of the *clint1* MO. Embryos injected with the *clint1*-atg MO plus TMRD exhibited localized epidermal aggregates in areas that contained TMRD (Fig. 5H), suggesting that a localized deficiency in Clint1 can cause localized cell aggregation. These aggregates were associated with neutrophil infiltration (Fig. 5H), suggesting that neutrophil recruitment is secondary to the localized epidermal defects.

To determine whether the epidermal proliferation in *clint1* morphants is a primary or secondary effect of the epithelial defects, a controlled number (2-4) of presumptive epidermal cells from *clint1* morphant or wild-type *Tg*(*β-actin:hras-eGFP*) embryos were transplanted into unlabeled wild-type recipients. Following transplantation at the shield stage, GFP-positive cells were counted at 2 and 3 dpf and expressed as average cell number per transplanted clone (see Fig. S6C in the supplementary material). Although *clint1* morphant cells often displayed rounder shapes than transplanted wild-type control cells, the average clone size was similar (see Fig. S6B,B′ in the supplementary material), suggesting that the epidermal hyperproliferation in non-mosaic *clint1* morphants and mutants is due to a non-cell-autonomous effect of the environment, such as a secondary consequence of the loss of epithelial homeostasis.

Clint1 and Lgl2 function synergistically to regulate epithelial homeostasis

To investigate potential defects in epithelial cell-cell adhesion, embryos were co-labeled with p63 and pan-cadherin antibodies. In *clint1* mutants, the epithelial organization of keratinocytes in areas of cell aggregation was disrupted, with overlapping cells (Fig. 6A′) and cell shedding (see Fig. 7). In epidermal aggregates, cadherin appeared to be localized to the membrane (Fig. 6A,A′), suggesting that cell-cell borders, although disorganized, were maintained.

Previous studies of *penner* (*lgl2*) mutant larvae have reported that mutant basal epidermal cells exhibit migratory behavior. Specifically, basal cells labeled with a pan-cytokeratin antibody are restricted to the dorsal and lateral epidermis in wild-type larvae but are found in the fin folds of *penner* mutants (Sonawane et al., 2005). To investigate this possibility in *clint1* mutants, larvae were immunolabeled with the pan-cytokeratin antibody. In wild-type larvae at 3 dpf, keratin expression appeared normal in the lateral epidermis (Fig. 6B) and included weak expression within the fin fold (Fig. 6C). We observed keratinocyte aggregation (Fig. 6B′-D′), with increased keratin staining in the fin folds of *clint1* mutants at 72 and 120 hpf (Fig. 6C′,D′). These findings indicate that the epidermal cells in *clint1* mutants exhibit defects similar to those reported for *penner* mutants.

To determine whether Clint1 and Lgl2 function synergistically to regulate epithelial homeostasis, low doses of MOs targeting both gene products were co-injected into wild-type embryos. Co-injection of *clint1*-ex1 and *lgl2* MOs produced severe epidermal defects more frequently (32%) than *clint1*-ex1 and control MO (<5%) or *lgl2* and control MO (<1%) co-injected embryos (Fig. 6F-I). This synergistic enhancement points to an interaction between *clint1* and *lgl2* in the regulation of epithelial homeostasis and morphology.

clint1 mutants have defects in hemidesmosome formation

As the primary defect of *penner* mutants is in hemidesmosome formation (Sonawane et al., 2005), we analyzed hemidesmosome formation in *clint1* mutants at 4 dpf by transmission electron

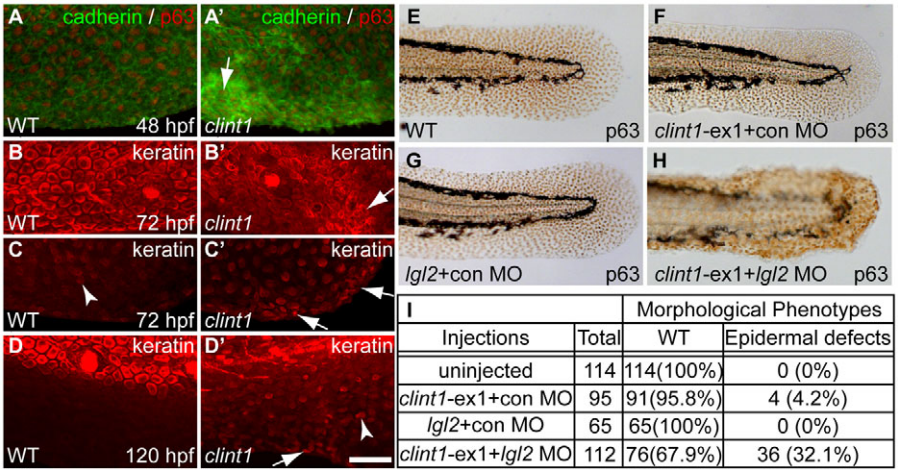

I

Injections	Total	Morphological Phenotypes	
		WT	Epidermal defects
uninjected	114	114(100%)	0 (0%)
clint1-ex1+con MO	95	91(95.8%)	4 (4.2%)
lgl2+con MO	65	65(100%)	0 (0%)
clint1-ex1+*lgl2* MO	112	76(67.9%)	36 (32.1%)

Fig. 6. Epidermal aggregation in *clint1* mutants and interaction with *lgl2*. (**A-D′**) Wild-type (A-D) and *clint1* mutant (A′-D′) zebrafish embryos staged at 48 (A,A′), 72 (B,C,B′,C′) and 120 (D,D′) hpf and immunolabeled for cadherin (green) and p63 (red) (A,A′) or for keratin (red) (B-D,B′-D′). Arrows (A′-D′) identify keratinocyte aggregation. Arrowheads (C,D′) identify keratin expression within fin folds. (**E-H**) p63 expression highlights epidermal morphology in uninjected (E), *clint1*-ex1 plus control MO (F), *lgl2* plus control MO (G), or *clint1*-ex1 plus *lgl2* MO (H) co-injected wild-type embryos. (**I**) Quantification of morphological phenotypes observed in E-H. Scale bar: 50 μm.

microscopy. Numerous electron-dense mature and immature hemidesmosomes were observed along the basal lamina of wild-type embryos, but few of these structures were observed in *clint1* mutant siblings (Fig. 7A,B,A′,B′). Other adhesive structures, such as desmosomes (Fig. 7C,C′) and tight junctions (Fig. 7D,D′), were unaffected in *clint1* mutants. Cellular fragmentation (Fig. 7A′,F) and shedding (Fig. 7C′) and nuclear condensation (Fig. 7E) were observed in epidermal cells of *clint1* mutants, which are consistent with the AO and BrdU labeling results documented above (Fig. 2; see Fig. S1 in the supplementary material). Furthermore, previous studies of *penner* mutants determined that Lgl2 regulates hemidesmosome formation through a Pkcζ-independent mechanism (Sonawane et al., 2009), and no differences were observed in transverse sections (see Fig. S6D,E in the supplementary material) or lateral views (data not shown) of the wild type and *clint1* mutants immunolabeled for Pkcζ. Thus, these data suggest that Clint1 and Lgl2 function synergistically to regulate hemidesmosome formation in the zebrafish epidermis using a Pkcζ-independent mechanism.

clint1 morphants display mesenchymal-like properties

For *penner* mutants, the aberrant keratin pattern suggested basal cell displacement. To study mesenchymal and migratory properties in *clint1* morphant cells, cell morphology and motility was assessed using cell transplants. Time-lapse confocal imaging was performed of basal keratinocytes in wild-type (wild-type donor into wild-type recipient) or *clint1* morphant environments (*clint1*-ex1 MO, *clint1* morphant donor into *clint1* morphant recipient) at 48 hpf (Fig. 8A-D; see Movies 5 and 6 in the supplementary material). Wild-type cells showed epithelial organization with stable cell-cell contacts and limited membrane protrusions and mobility during the 90-minute time-lapse movie (Fig. 8A,C; see Movie S5 in the supplementary material; in 8/8 movies). By contrast, *clint1* morphant cells displayed mesenchymal morphology and behavior with fibroblastoid cell shapes and transient loss of cell-cell contacts. They also exhibited increased protrusive activity (data not shown) and significant migratory behavior (Fig. 6B,D; see Movie 6 in the supplementary material; in 4/6 movies). These findings suggest that loss of Clint1 impairs epithelial cell-cell contacts and causes keratinocytes to acquire mesenchymal properties characterized by increased motility.

DISCUSSION

Clint1 is a novel regulator of epidermal homeostasis and hemidesmosome formation

Previous studies have reported an important role for Clint1 in vesicle transport; however, an in vivo function has not been reported to date. Here, we identify Clint1 as a novel regulator of epidermal homeostasis that is required for embryonic survival in the zebrafish. Clint1 is expressed in keratinocytes and localizes to intracellular vesicles. The epidermis of *clint1* mutants displays hyperproliferation and cell death by 36 hpf and inflammation by 48 hpf. The defects in *clint1* mutants can be rescued by injection of *clint1* mRNA and are phenocopied by *clint1* MOs. Electron micrographs show that tight junctions and desmosomes are intact, but hemidesmosome formation is impaired in *clint1* mutants. The lateral epidermis appears disorganized, with protruding epidermal cells, and keratinized cells appear in the fin fold, suggestive of epidermal displacement related to EMT. Time-lapse movies of *clint1* morphants show enhanced protrusive activity and mobility of epidermal cells. Taken together, our findings suggest that Clint1 is indispensable for epidermal homeostasis. Furthermore, the findings indicate that a deficiency of Clint1 induces a phenotype that resembles the human condition psoriasis.

Comparison of *clint1* mutants with other *psoriasis*-like mutants

Recent progress has been made in defining pathways that regulate epidermal integrity and function. The identification of mutants with psoriasis-like phenotypes, such as *penner* (Sonawane et al., 2005), *psoriasis* (Webb et al., 2008) and *hai1* (Carney et al., 2007; Mathias et al., 2007), has provided clues as to the genetic program of epidermal development in zebrafish. A crucial component of these epidermal phenotypes is keratinocyte hyperproliferation and the development of epidermal aggregates. Comparison of these phenotypes with those observed in *clint1* mutants suggests potential relationships between these signaling pathways.

Previous work has suggested a link between epithelial hyperproliferation and the regulation of epithelial polarity. An example of this connection is the association between mutations in the polarity gene *lgl2* and the development of hyperproliferation of epithelial cells in *Drosophila* (Bilder, 2004) and zebrafish (Sonawane et al., 2005; Vasioukhin, 2006). Previous studies have suggested a possible role for Clint1 in the regulation of cell polarity through a proposed interaction between the ENTH domain of Clint1

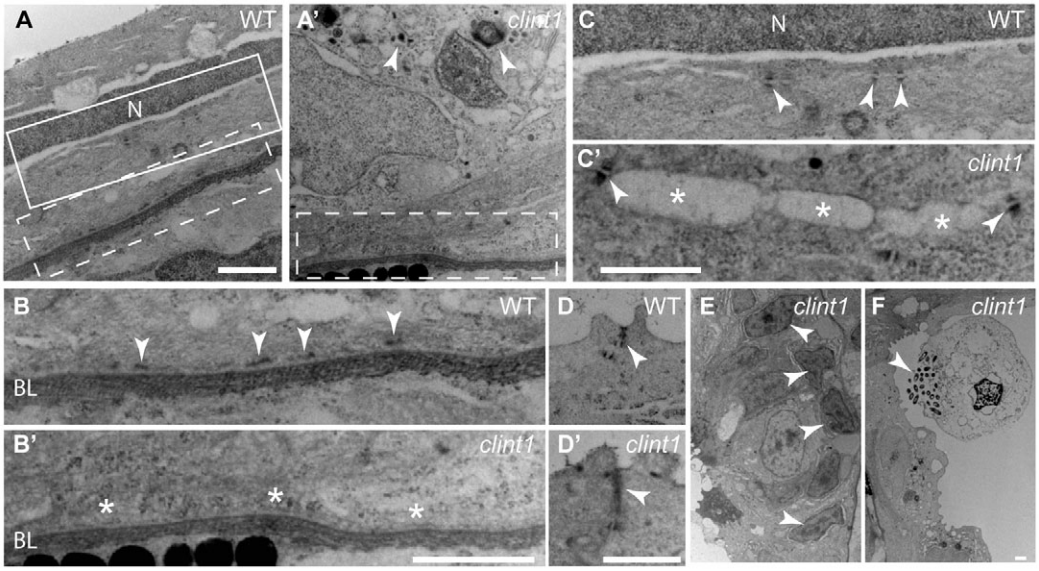

Fig. 7. Impaired hemidesmosome formation in *clint1* mutants. Transmission electron micrographs of transverse sections of wild-type (**A-D**) and *clint1* mutant (**A′-D′**,**E**,**F**) zebrafish embryos staged at 4 dpf. The dashed boxed regions in A and A′ are magnified in B and B′, respectively. The solid boxed region in A is magnified in C. Arrowheads label hemidesmosomes (B), desmosomes (C,C′), tight junctions (D,D′), cellular fragmentation (A′,F) and condensed nuclei (E). Asterisks highlight absence of hemidesmosomes (B′) and detachment of epidermal cells (C′). N, nucleus; BL, basal lamina. Scale bars: 1 μm.

and the GTPase-activating proteins (GAPs) for Cdc42 (Aguilar et al., 2006; Ritter and McPherson, 2006). Cytokeratin is an early polarity marker in zebrafish that displays basal localization of keratin filaments at 3 dpf (Sonawane et al., 2005). In *penner* mutants, cytokeratin is not restricted to the basal cortex, suggesting a loss of polarity, and ectopic expression of cytokeratin is suggestive of EMT. Although cytokeratin staining did not indicate polarity defects (data not shown), a similar pattern of ectopic keratin expression was observed within the fin fold of *clint1* mutants at 5 dpf, suggesting EMT. Finally, defects in hemidesmosome formation were evident in electron micrographs of both *penner* (Sonawane et al., 2005) and *clint1* mutants. A recent report on the *penner* mutant suggests that Lgl2 functions antagonistically with E-cadherin to regulate hemidesmosome formation through a Pkcζ-independent mechanism (Sonawane et al., 2009). Although the relationship between Clint1 and E-cadherin remains unclear, Pkcζ staining in *clint1* mutants also suggests that Clint1 regulates hemidesmosome formation through a Pkcζ-independent mechanism. Our findings support an interaction between *lgl2* and *clint1* in the regulation of epidermal homeostasis and hemidesmosome formation.

The mechanism by which these two pathways interact remains unknown; however, both Clint1 (Hirst et al., 2004; Miller et al., 2007; Chidambaram et al., 2008) and Lgl2 (Musch et al., 2002) interact with SNARE proteins, such as syntaxins, providing a potential link between the two pathways. Based on recent reports, Vti1b was an obvious candidate to regulate epidermal homeostasis. Zebrafish Vti1b and Clint1 were found to co-localize at intracellular vesicles. However, no epidermal phenotypes were observed in *vti1b*-deficient embryos, and a functional interaction was not observed between Clint1 and Vti1b (data not shown). Taken together, our findings suggest that Clint1 regulates epithelial homeostasis through a vesicle transport pathway that functions synergistically with Lgl2.

Cadherins are transmembrane linker proteins that mediate cell-cell contacts. In *clint1* mutants, cell-cell contacts were disrupted in areas of epithelial aggregation, but cadherin surface expression at cell-cell contacts appeared normal, similar to reports for the *psoriasis* mutant (Webb et al., 2008). Similarly, apical cell-cell junctions also appeared to be intact in *penner* mutants by β-catenin staining at lateral-apical cell-cell junctions (Sonawane et al., 2005). Other similarities between *clint1* and *psoriasis* mutants include persistent hyperproliferation that continues beyond 120 hpf and the non-cell-autonomous nature of the epidermal proliferation defects. However, in contrast to *penner* and *clint1* mutants, the *psoriasis* mutant displays impaired epidermal development related to the differential expression of keratin genes, suggesting a potentially different mode of action. Future studies will be needed to identify the causal mutation of *psoriasis* mutants and to investigate potential interactions with Clint1 in regulating epidermal homeostasis.

Finally, comparison of *clint1* and *hai1* mutants also highlights similarities. Epithelial cells in *clint1* mutants displayed transient losses of cell-cell contacts and exhibited mesenchymal-like characteristics with single-cell motility, as reported with *hai1* mutants (Carney et al., 2007). Further studies are needed to address possible differences in mesenchymal behaviors in the different zebrafish mutants. It appears that partial or complete EMT may be a common feature of *psoriasis*-like mutants in zebrafish and might contribute to the epithelial aggregation observed in these mutants.

Inflammation in *clint1* mutants

The human condition psoriasis is characterized by epithelial proliferation and inflammation of the skin (Bowcock and Krueger, 2005; Lowes et al., 2007). Similar to *clint1* mutants, zebrafish *hai1* mutants exhibited hyperproliferation and inflammation involving neutrophils and macrophages (Mathias et al., 2007). Leukocytes were observed in similar locations in *hai1* and *clint1* mutants. The persistent inflammation in *hai1* mutants was characterized by leukocyte recruitment into the fin in the absence of reverse migration back to the vasculature, suggesting that the persistent inflammation might, in part, be due to impaired resolution. By contrast, leukocyte

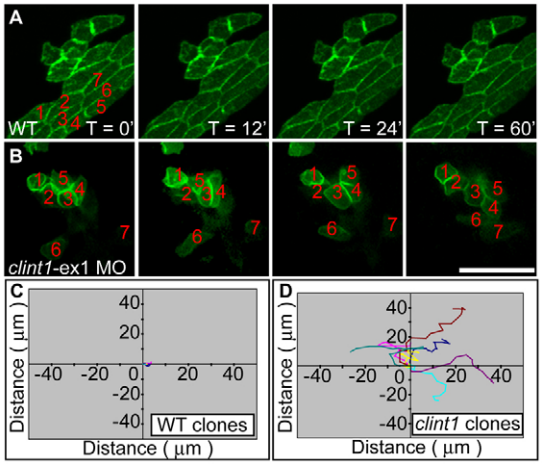

Fig. 8. Mesenchymal behavior of epidermal cells in *clint1* mutants. (**A**,**B**) Still images from in vivo time-lapse microscopy of keratinocyte clusters from uninjected (A) (see Movie 5 in the supplementary material) or *clint1*-ex1 MO-injected (B) (see Movie 6 in the supplementary material) *Tg*(*β-actin:hras-eGFP*) zebrafish embryos that were transplanted into ventral ectoderm of non-transgenic wild-type (A) or *clint1* morphant (B) embryos, respectively. Epidermal cells from *clint1* morphants exhibit loss of cell-cell contacts and increased motility (B,D). Note the change in position of the numbered cells in B. (**C**,**D**) Quantification of migration of the numbered GFP-positive keratinocytes in unlabeled wild type (C) (see Movie 5 in the supplementary material) or *clint1*-morphant recipients (D) (see Movie 6 in the supplementary material). Scale bar: 50 μm.

trafficking in the *clint1* mutants showed robust bidirectional trafficking between the fin folds and the vasculature, suggesting that reverse migration remains intact. In both *clint1* and *hai1* mutants, individual neutrophil migration was characterized by periods of motility alternating with frequent pauses, although pausing was more frequent in *clint1* mutants, a likely reflection of differences in phenotypic severity.

The recruitment signals responsible for persistent leukocyte infiltration remain unknown. Candidate factors include the inflammatory cytokine *il1b*, expression of which is increased in *clint1* mutants. However, *il1b* alone did not appear to be sufficient to induce the inflammatory response because an *il1b*-specific MO did not block inflammatory cell recruitment in the *clint1* mutants (data not shown). Alternatively, inflammation can be induced by dying cells in order to allow for clearance of cellular debris. Although caspase inhibitors did not affect the leukocyte infiltration (data not shown), we cannot rule out the possibility that tissue damage signals contribute to leukocyte recruitment in the *clint1* mutant. In support of this possibility, removal of tissue debris by phagocytic cells was observed in the *clint1* mutants. Another potential target is Toll-like receptor (TLR) signaling, as Tlr3 was recently implicated as an endogenous sensor of tissue necrosis during acute inflammation (Cavassani et al., 2008). It is also possible that one of these factors alone is not sufficient for leukocyte infiltration in *clint1* mutants, and that inhibition of multiple pathways might be necessary to limit the inflammatory response.

EMT and leukocyte infiltration

A deficiency of either Clint1 or Hai1 leads to a phenotype characterized by epithelial proliferation, EMT and leukocyte infiltration, similar to a wound response. Although leukocyte infiltration has not been assessed in all zebrafish epidermal mutants, evidence indicates that EMT and/or a loss of epithelial integrity would be accompanied by inflammation. In accordance with this possibility, a recent study reported that loss of epidermal Caspase 8 induces a wound healing response characterized by epidermal hyperproliferation, apoptosis and inflammation (Lee et al., 2009), similar to the phenotype of the *clint1* mutant. Further studies are needed to examine the relationship between inflammation and EMT in zebrafish models, and to investigate the ability of leukocyte infiltration to exacerbate the EMT phenotype.

In summary, *clint1* is an essential gene for the regulation of epidermal homeostasis in zebrafish. Importantly, this is the first reported in vivo function for Clint1 in an animal model. The findings suggest that Clint1 deficiency results in a phenotype that resembles the human condition psoriasis. It is of substantial importance to identify model systems that are amenable to drug screening and that can provide insight into the factors that contribute to inflammation in response to damaged tissues, or in the context of proliferative epidermal tissues. The *clint1* mutant will provide a powerful tool with which to dissect the pathways that regulate epidermal homeostasis and contribute to the onset and resolution of inflammatory responses.

Acknowledgements
We gratefully acknowledge Adam Amsterdam and Nancy Hopkins (M.I.T.) for providing *hi1520* mutants, Satoshi Kinoshita for zebrafish sections, Ben August for electron microscopy, Sa Kan Yoo for thoughtful discussions and Andrea Gallagher for technical assistance. This work was supported by NIH grants to A.H. (R01 GM074827), J.R. (5KO1DK69672) and by an Arthritis Foundation fellowship (J.R.M.) and Hematology training grant (M.E.D.). M.H. and J.H. thank the Max-Planck society for initial support. Deposited in PMC for release after 12 months.

Competing interests statement
The authors declare no competing interests.

Supplementary material
Supplementary material for this article is available at
http://dev.biologists.org/cgi/content/full/136/15/2591/DC1

References
Aguilar, R. C., Longhi, S. A., Shaw, J. D., Yeh, L. Y., Kim, S., Schon, A., Freire, E., Hsu, A., McCormick, W. K., Watson, H. A. et al. (2006). Epsin N-terminal homology domains perform an essential function regulating Cdc42 through binding Cdc42 GTPase-activating proteins. *Proc. Natl. Acad. Sci. USA* **103**, 4116-4121.
Amsterdam, A. and Hopkins, N. (2004). Retroviral-mediated insertional mutagenesis in zebrafish. *Methods Cell Biol.* **77**, 3-20.
Amsterdam, A., Burgess, S., Golling, G., Chen, W., Sun, Z., Townsend, K., Farrington, S., Haldi, M. and Hopkins, N. (1999). A large-scale insertional mutagenesis screen in zebrafish. *Genes Dev.* **13**, 2713-2724.
Amsterdam, A., Nissen, R. M., Sun, Z., Swindell, E. C., Farrington, S. and Hopkins, N. (2004). Identification of 315 genes essential for early zebrafish development. *Proc. Natl. Acad. Sci. USA* **101**, 12792-12797.
Bakkers, J., Hild, M., Kramer, C., Furutani-Seiki, M. and Hammerschmidt, M. (2002). Zebrafish DeltaNp63 is a direct target of Bmp signaling and encodes a transcriptional repressor blocking neural specification in the ventral ectoderm. *Dev. Cell* **2**, 617-627.
Bennett, C. M., Kanki, J. P., Rhodes, J., Liu, T. X., Paw, B. H., Kieran, M. W., Langenau, D. M., Delahaye-Brown, A., Zon, L. I., Fleming, M. D. et al. (2001). Myelopoiesis in the zebrafish, Danio rerio. *Blood* **98**, 643-651.
Bilder, D. (2004). Epithelial polarity and proliferation control: links from the Drosophila neoplastic tumor suppressors. *Genes Dev.* **18**, 1909-1925.
Bowcock, A. M. and Krueger, J. G. (2005). Getting under the skin: the immunogenetics of psoriasis. *Nat. Rev. Immunol.* **5**, 699-711.
Carney, T. J., von der Hardt, S., Sonntag, C., Amsterdam, A., Topczewski, J., Hopkins, N. and Hammerschmidt, M. (2007). Inactivation of serine protease Matriptase1a by its inhibitor Hai1 is required for epithelial integrity of the zebrafish epidermis. *Development* **134**, 3461-3471.
Carradice, D. and Lieschke, G. J. (2008). Zebrafish in hematology: sushi or science? *Blood* **111**, 3331-3342.

Cavassani, K. A., Ishii, M., Wen, H., Schaller, M. A., Lincoln, P. M., Lukacs, N. W., Hogaboam, C. M. and Kunkel, S. L. (2008). TLR3 is an endogenous sensor of tissue necrosis during acute inflammatory events. *J. Exp. Med.* **205**, 2609-2621.

Chen, W., Burgess, S., Golling, G., Amsterdam, A. and Hopkins, N. (2002). High-throughput selection of retrovirus producer cell lines leads to markedly improved efficiency of germ line-transmissible insertions in zebra fish. *J. Virol.* **76**, 2192-2198.

Chidambaram, S., Zimmermann, J. and von Mollard, G. F. (2008). ENTH domain proteins are cargo adaptors for multiple SNARE proteins at the TGN endosome. *J. Cell Sci.* **121**, 329-338.

Chua, K. L. and Lim, T. M. (2000). Type I and type II cytokeratin cDNAs from the zebrafish (Danio rerio) and expression patterns during early development. *Differentiation* **66**, 31-41.

Cooper, M. S., Szeto, D. P., Sommers-Herivel, G., Topczewski, J., Solnica-Krezel, L., Kang, H. C., Johnson, I. and Kimelman, D. (2005). Visualizing morphogenesis in transgenic zebrafish embryos using BODIPY TR methyl ester dye as a vital counterstain for GFP. *Dev. Dyn.* **232**, 359-368.

Davis, J. M., Clay, H., Lewis, J. L., Ghori, N., Herbomel, P. and Ramakrishnan, L. (2002). Real-time visualization of mycobacterium-macrophage interactions leading to initiation of granuloma formation in zebrafish embryos. *Immunity* **17**, 693-702.

de Jong, J. L. and Zon, L. I. (2005). Use of the zebrafish system to study primitive and definitive hematopoiesis. *Annu. Rev. Genet.* **39**, 481-501.

Doan, A. T. and Huttenlocher, A. (2007). RACK1 regulates Src activity and modulates paxillin dynamics during cell migration. *Exp. Cell Res.* **313**, 2667-2679.

Hall, C., Flores, M. V., Storm, T., Crosier, K. and Crosier, P. (2007). The zebrafish lysozyme C promoter drives myeloid-specific expression in transgenic fish. *BMC Dev. Biol.* **7**, 42.

Hammerschmidt, M., Pelegri, F., Mullins, M. C., Kane, D. A., van Eeden, F. J., Granato, M., Brand, M., Furutani-Seiki, M., Haffter, P., Heisenberg, C. P. et al. (1996). dino and mercedes, two genes regulating dorsal development in the zebrafish embryo. *Development* **123**, 95-102.

Hirst, J., Miller, S. E., Taylor, M. J., von Mollard, G. F. and Robinson, M. S. (2004). EpsinR is an adaptor for the SNARE protein Vti1b. *Mol. Biol. Cell* **15**, 5593-5602.

Hsu, K., Traver, D., Kutok, J. L., Hagen, A., Liu, T. X., Paw, B. H., Rhodes, J., Berman, J. N., Zon, L. I., Kanki, J. P. et al. (2004). The pu.1 promoter drives myeloid gene expression in zebrafish. *Blood* **104**, 1291-1297.

Imboden, M., Goblet, C., Korn, H. and Vriz, S. (1997). Cytokeratin 8 is a suitable epidermal marker during zebrafish development. *C. R. Acad. Sci. III* **320**, 689-700.

Kalthoff, C., Groos, S., Kohl, R., Mahrhold, S. and Ungewickell, E. J. (2002). Clint: a novel clathrin-binding ENTH-domain protein at the Golgi. *Mol. Biol. Cell* **13**, 4060-4073.

Kimmel, C. B., Ballard, W. W., Kimmel, S. R., Ullmann, B. and Schilling, T. F. (1995). Stages of embryonic development of the zebrafish. *Dev. Dyn.* **203**, 253-310.

Le Guellec, D., Morvan-Dubois, G. and Sire, J. Y. (2004). Skin development in bony fish with particular emphasis on collagen deposition in the dermis of the zebrafish (Danio rerio). *Int. J. Dev. Biol.* **48**, 217-231.

Lee, H. and Kimelman, D. (2002). A dominant-negative form of p63 is required for epidermal proliferation in zebrafish. *Dev. Cell* **2**, 607-616.

Lee, P., Lee, D. J., Chan, C., Chen, S. W., Ch'en, I. and Jamora, C. (2009). Dynamic expression of epidermal caspase 8 simulates a wound healing response. *Nature* **458**, 519-523.

Lieschke, G. J., Oates, A. C., Crowhurst, M. O., Ward, A. C. and Layton, J. E. (2001). Morphologic and functional characterization of granulocytes and macrophages in embryonic and adult zebrafish. *Blood* **98**, 3087-3096.

Lowes, M. A., Bowcock, A. M. and Krueger, J. G. (2007). Pathogenesis and therapy of psoriasis. *Nature* **445**, 866-873.

Martorana, M. L., Tawk, M., Lapointe, T., Barre, N., Imboden, M., Joulie, C., Geraudie, J. and Vriz, S. (2001). Zebrafish keratin 8 is expressed at high levels in the epidermis of regenerating caudal fin. *Int. J. Dev. Biol.* **45**, 449-452.

Mathias, J. R., Perrin, B. J., Liu, T. X., Kanki, J., Look, A. T. and Huttenlocher, A. (2006). Resolution of inflammation by retrograde chemotaxis of neutrophils in transgenic zebrafish. *J. Leukoc. Biol.* **80**, 1281-1288.

Mathias, J. R., Dodd, M. E., Walters, K. B., Rhodes, J., Kanki, J. P., Look, A. T. and Huttenlocher, A. (2007). Live imaging of chronic inflammation caused by mutation of zebrafish Hai1. *J. Cell Sci.* **120**, 3372-3383.

Meijer, A. H., van der Sar, A. M., Cunha, C., Lamers, G. E., Laplante, M. A., Kikuta, H., Bitter, W., Becker, T. S. and Spaink, H. P. (2008). Identification and real-time imaging of a myc-expressing neutrophil population involved in inflammation and mycobacterial granuloma formation in zebrafish. *Dev. Comp. Immunol.* **32**, 36-49.

Miller, S. E., Collins, B. M., McCoy, A. J., Robinson, M. S. and Owen, D. J. (2007). A SNARE-adaptor interaction is a new mode of cargo recognition in clathrin-coated vesicles. *Nature* **450**, 570-574.

Mills, I. G., Praefcke, G. J., Vallis, Y., Peter, B. J., Olesen, L. E., Gallop, J. L., Butler, P. J., Evans, P. R. and McMahon, H. T. (2003). EpsinR: an AP1/clathrin interacting protein involved in vesicle trafficking. *J. Cell Biol.* **160**, 213-222.

Musch, A., Cohen, D., Yeaman, C., Nelson, W. J., Rodriguez-Boulan, E. and Brennwald, P. J. (2002). Mammalian homolog of Drosophila tumor suppressor lethal (2) giant larvae interacts with basolateral exocytic machinery in Madin-Darby canine kidney cells. *Mol. Biol. Cell* **13**, 158-168.

Nuesslein-Volhard, C. and Dahm, R. (2002). *Zebrafish, A Practical Approach*. New York: Oxford University Press.

Pressley, M. E., Phelan, P. E., 3rd, Witten, P. E., Mellon, M. T. and Kim, C. H. (2005). Pathogenesis and inflammatory response to Edwardsiella tarda infection in the zebrafish. *Dev. Comp. Immunol.* **29**, 501-513.

Renshaw, S. A., Loynes, C. A., Trushell, D. M., Elworthy, S., Ingham, P. W. and Whyte, M. K. (2006). A transgenic zebrafish model of neutrophilic inflammation. *Blood* **108**, 3976-3978.

Rhodes, J., Hagen, A., Hsu, K., Deng, M., Liu, T. X., Look, A. T. and Kanki, J. P. (2005). Interplay of pu.1 and gata1 determines myelo-erythroid progenitor cell fate in zebrafish. *Dev. Cell* **8**, 97-108.

Ritter, B. and McPherson, P. S. (2006). There's a GAP in the ENTH domain. *Proc. Natl. Acad. Sci. USA* **103**, 3953-3954.

Sonawane, M., Carpio, Y., Geisler, R., Schwarz, H., Maischein, H. M. and Nuesslein-Volhard, C. (2005). Zebrafish penner/lethal giant larvae 2 functions in hemidesmosome formation, maintenance of cellular morphology and growth regulation in the developing basal epidermis. *Development* **132**, 3255-3265.

Sonawane, M., Martin-Maischein, H., Schwarz, H. and Nusslein-Volhard, C. (2009). Lgl2 and E-cadherin act antagonistically to regulate hemidesmosome formation during epidermal development in zebrafish. *Development* **136**, 1231-1240.

Thisse, B. and Thisse, C. (2004). Fast release clones: a high throughput expression analysis. ZFIN Direct Data Submission, http://zfin.org.

Tingaud-Sequeira, A., Forgue, J., Andre, M. and Babin, P. J. (2006). Epidermal transient down-regulation of retinol-binding protein 4 and mirror expression of apolipoprotein Eb and estrogen receptor 2a during zebrafish fin and scale development. *Dev. Dyn.* **235**, 3071-3079.

van der Sar, A. M., Musters, R. J., van Eeden, F. J., Appelmelk, B. J., Vandenbroucke-Grauls, C. M. and Bitter, W. (2003). Zebrafish embryos as a model host for the real time analysis of Salmonella typhimurium infections. *Cell. Microbiol.* **5**, 601-611.

Vasioukhin, V. (2006). Lethal giant puzzle of Lgl. *Dev. Neurosci.* **28**, 13-24.

Walters, K. B., Dodd, M. E., Mathias, J. R., Gallagher, A. J., Bennin, D. A., Rhodes, J., Kanki, J. P., Look, A. T., Grinblat, Y. and Huttenlocher, A. (2009). Muscle degeneration and leukocyte infiltration caused by mutation of zebrafish Fad24. *Dev. Dyn.* **238**, 86-99.

Wasiak, S., Legendre-Guillemin, V., Puertollano, R., Blondeau, F., Girard, M., de Heuvel, E., Boismenu, D., Bell, A. W., Bonifacino, J. S. and McPherson, P. S. (2002). Enthoprotin: a novel clathrin-associated protein identified through subcellular proteomics. *J. Cell Biol.* **158**, 855-862.

Webb, A. E., Sanderford, J., Frank, D., Talbot, W. S., Driever, W. and Kimelman, D. (2007). Laminin alpha5 is essential for the formation of the zebrafish fins. *Dev. Biol.* **311**, 369-382.

Webb, A. E., Driever, W. and Kimelman, D. (2008). psoriasis regulates epidermal development in zebrafish. *Dev. Dyn.* **237**, 1153-1164.

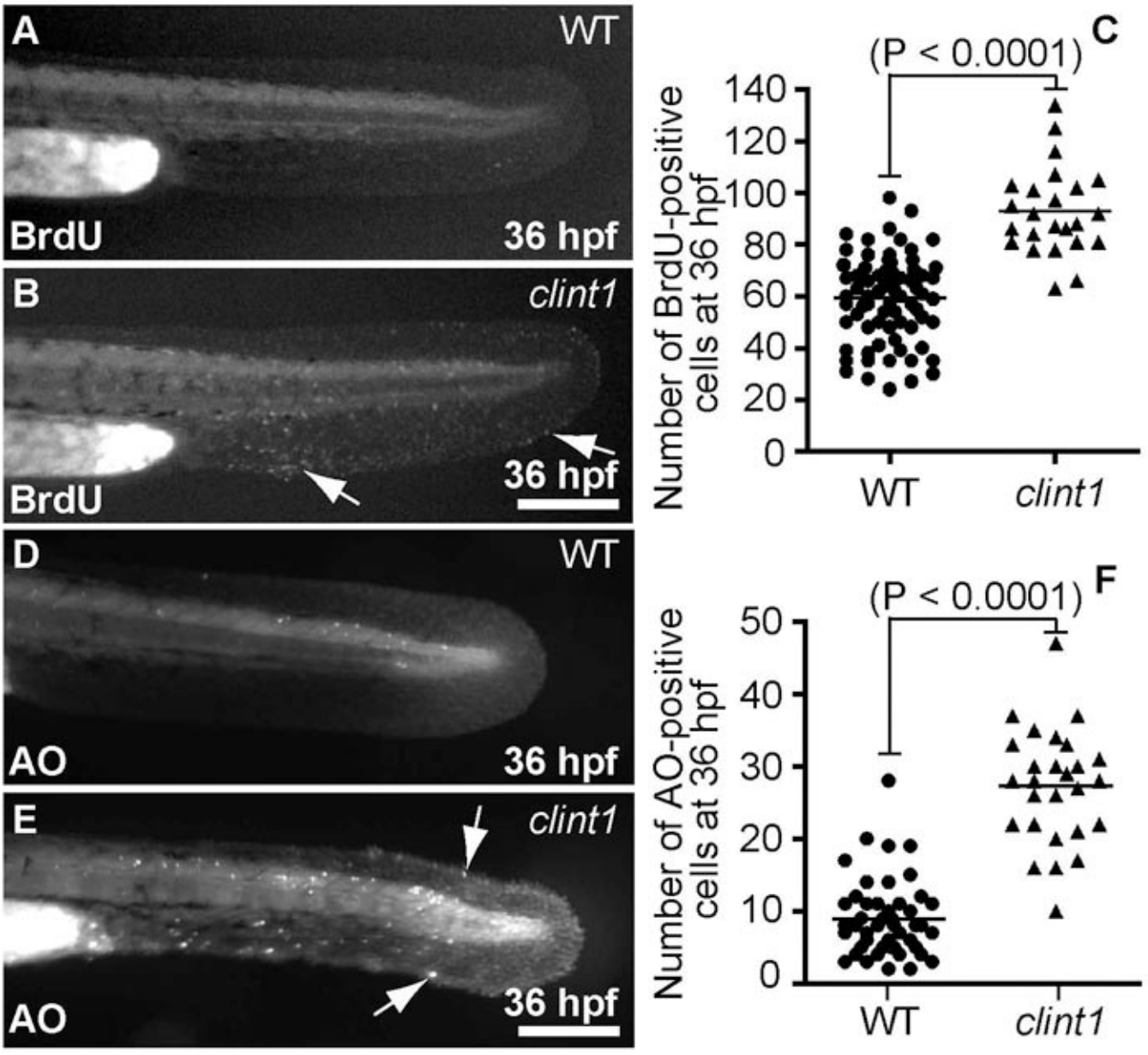
A
WT
BrdU
36 hpf
B
clint1
BrdU
36 hpf
C
(P < 0.0001)
Number of BrdU-positive cells at 36 hpf
140
120
100
80
60
40
20
0
WT
clint1
D
WT
AO
36 hpf
E
clint1
AO
36 hpf
F
(P < 0.0001)
Number of AO-positive cells at 36 hpf
50
40
30
20
10
0
WT
clint1

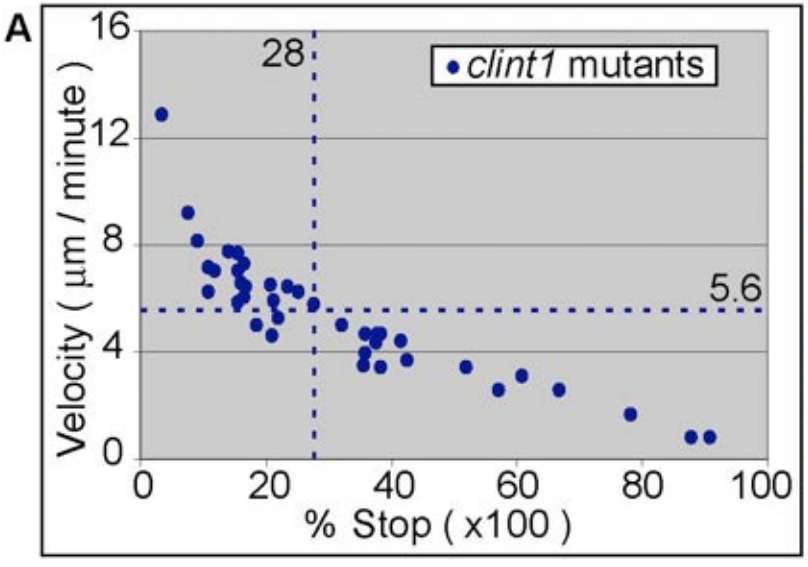

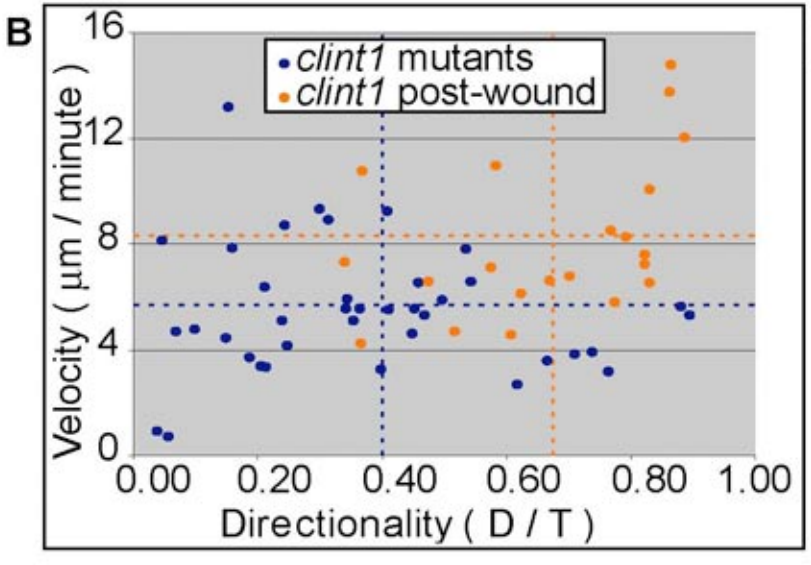

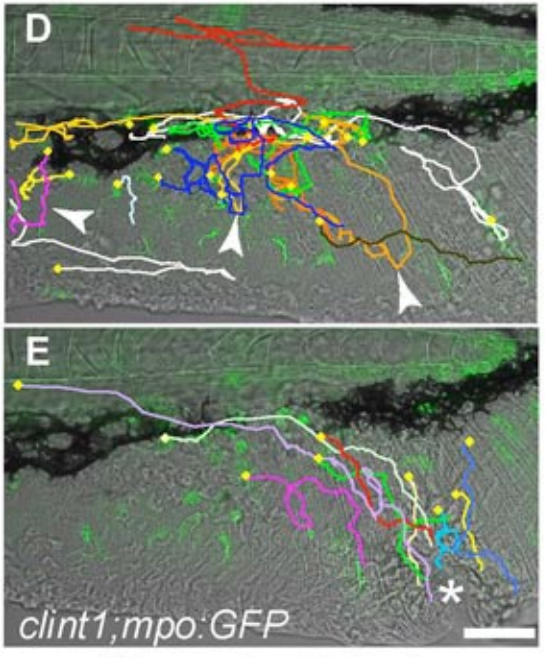

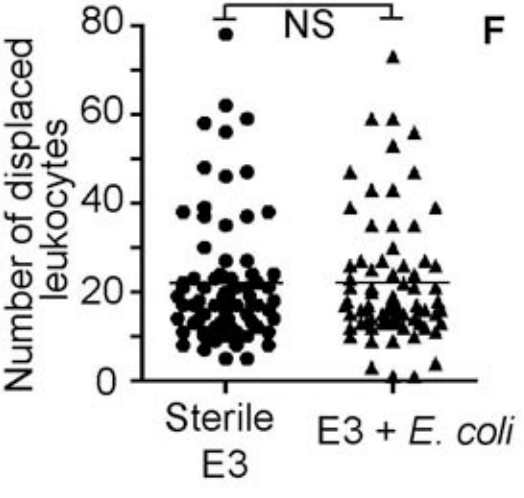

C	Cells	Velocity (µm/min)	Directionality (D/T)
clint1 mutants	39	5.7 (+/- 0.43)	0.4 (+/- 0.06)
clint1 post-wound	22	8.3(+/- 2.5)	0.67 (+/- 0.04)

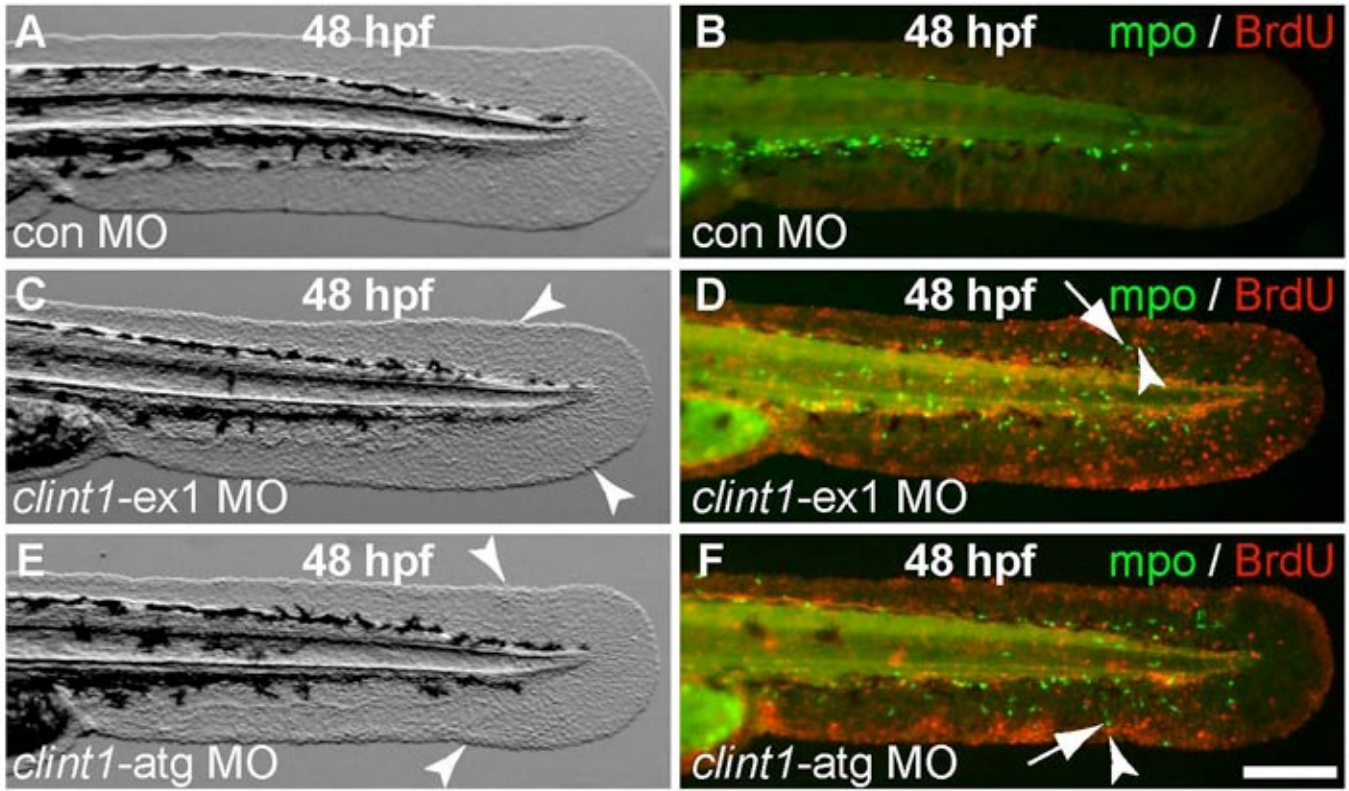
A
48 hpf
con MO
B
48 hpf
mpo / BrdU
con MO
C
48 hpf
clint1-ex1 MO
D
48 hpf
mpo / BrdU
clint1-ex1 MO
E
48 hpf
clint1-atg MO
F
48 hpf
mpo / BrdU
clint1-atg MO

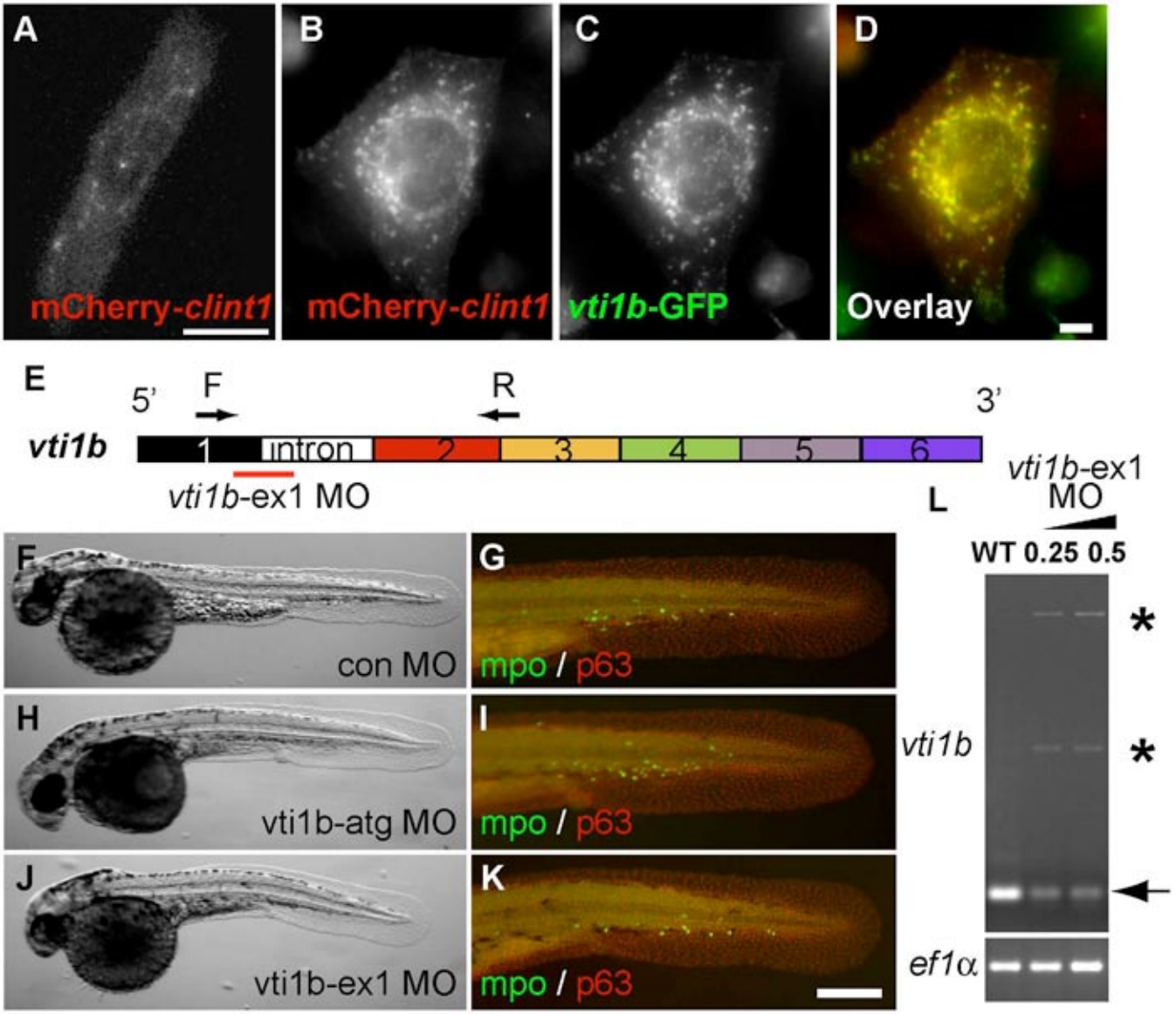
A
mCherry-clint1
B
mCherry-clint1
C
vti1b-GFP
D
Overlay
E
5'
F
R
3'
vti1b
1
intron
2
3
4
5
6
vti1b-ex1 MO
F
con MO
G
mpo / p63
H
vti1b-atg MO
I
mpo / p63
J
vti1b-ex1 MO
K
mpo / p63
L
vti1b-ex1 MO
WT 0.25 0.5
vti1b
ef1α

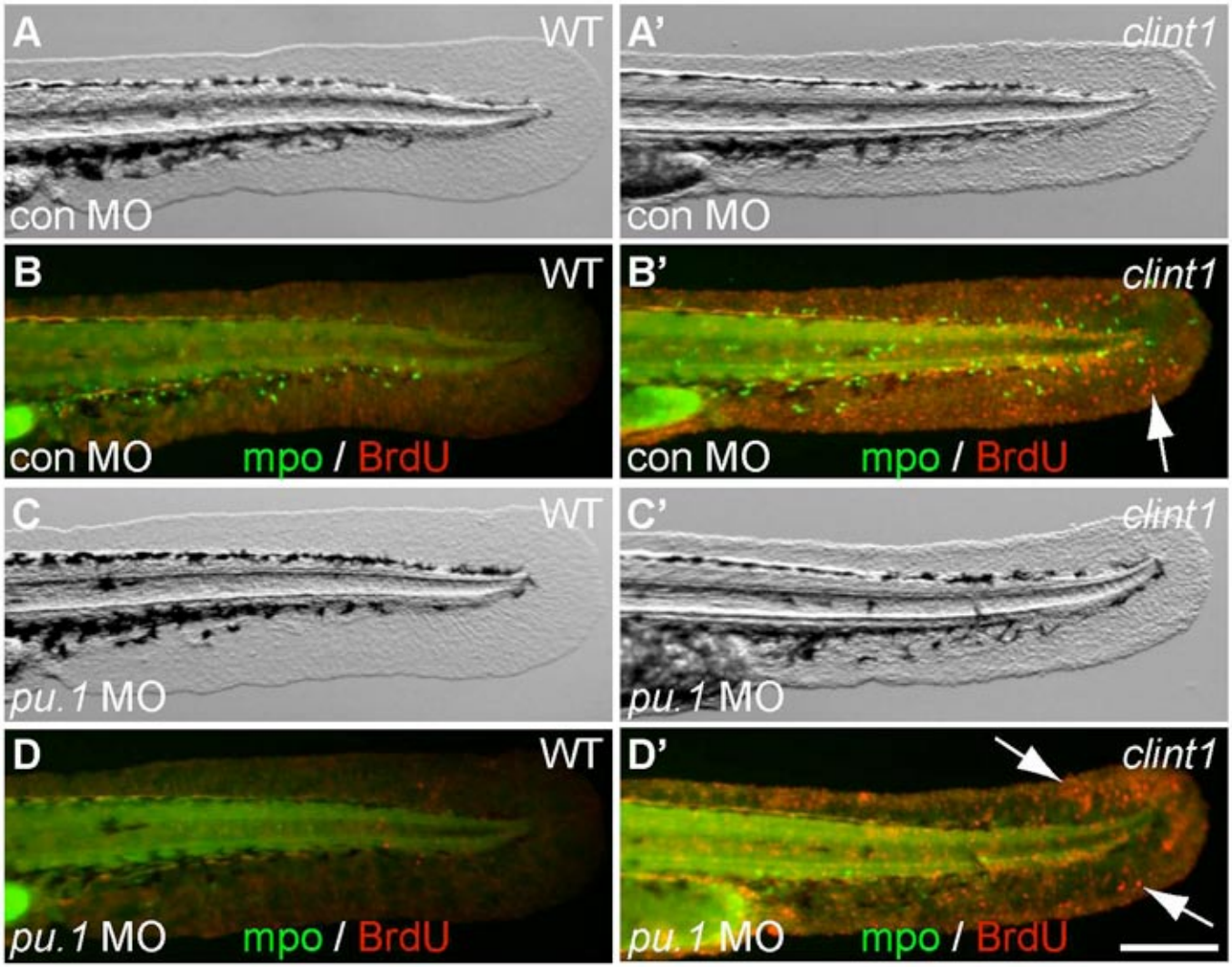
A
WT
con MO
A'
clint1
con MO
B
WT
con MO
mpo / BrdU
B'
clint1
con MO
mpo / BrdU
C
WT
pu.1 MO
C'
clint1
pu.1 MO
D
WT
pu.1 MO
mpo / BrdU
D'
clint1
pu.1 MO
mpo / BrdU

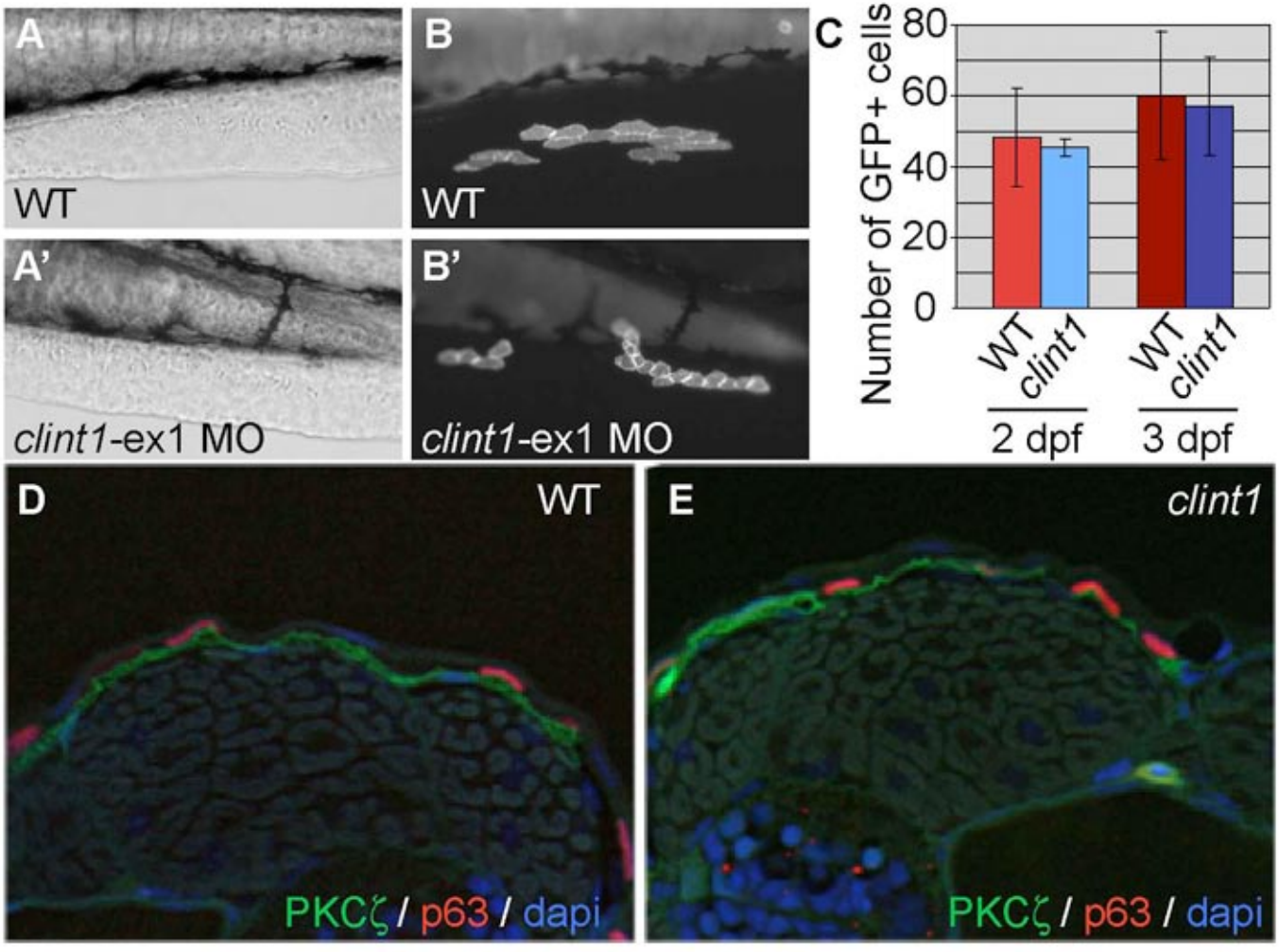
A
WT
B
WT
A'
clint1-ex1 MO
B'
clint1-ex1 MO
C
Number of GFP+ cells
80
60
40
20
0
WT
clint1
WT
clint1
2 dpf
3 dpf
D
WT
PKCζ / p63 / dapi
E
clint1
PKCζ / p63 / dapi